From graphene to graphite: Electronic structure around the *K* point

B. Partoens* and F. M. Peeters†
Universiteit Antwerpen, Departement Fysica, Groenenborgerlaan 171, B-2020 Antwerpen, Belgium
(Received 15 March 2006; revised manuscript received 7 June 2006; published 2 August 2006)

Within a tight-binding approach we investigate how the electronic structure evolves from a single graphene layer into bulk graphite by computing the band structure of one, two, and three layers of graphene. It is well known that a single graphene layer is a zero-gap semiconductor with a linear Dirac-like spectrum around the Fermi energy, while graphite shows a semimetallic behavior with a band overlap of about 41 meV. In contrast to a single graphene layer, we show that two graphene layers have a parabolic spectrum around the Fermi energy and are a semimetal like graphite; however, the band overlap of 0.16 meV is extremely small. Three and more graphene layers show a clear semimetallic behavior. For 11 and more layers the difference in band overlap with graphite is smaller than 10%.

DOI: 10.1103/PhysRevB.74.075404 PACS number(s): 81.05.Uw, 73.63.Bd, 73.43.Cd

I. INTRODUCTION

Graphite consists of van der Waals coupled graphene layers.[1] Graphene is a layer of carbon atoms with hexagonal symmetry. In graphite every other layer of graphene is shifted in the horizontal plane, leading to the well-known *AB* stacking.

Recently, one succeeded in obtaining stable multilayers and even single layers of graphene.[2] Because of the weak interlayer coupling, it is surprising that a single graphene layer shows very different transport properties than systems consisting of two or more graphene layers. As the charge carriers in such thin graphene films are confined to two dimensions, one has looked for and observed the quantum Hall effect. However, in the case of a single graphene layer, its behavior differs drastically from the well-studied case of quantum wells in conventional semiconductor interfaces; i.e., a half-integer quantum Hall effect was observed.[3,4] This half-integer quantum Hall effect is due to the existence of both electronlike and holelike Landau states at zero energy.[5,6] The system consisting of two layers of graphene does not show this half-integer quantum Hall effect[3] (however, another anomaly—a double step—is theoretically predicted[7] and observed experimentally[8]).

It is also well known that a single graphene layer is a zero-gap semiconductor while graphite is a semimetal. Therefore it is interesting to investigate how the electronic structure changes as a function of the number of graphene layers and how many layers one needs to observe the bulk graphite behavior. We will concentrate on an accurate determination of the band structure near the Fermi energy. To realize this, we apply the tight-binding approach. All results in this paper are verified by *ab initio* density-functional theory calculations in the local density approximation, but the advantage of the tight-binding approach is that the Hamiltonian for a general number of graphene layers can be and is explicitly given and can therefore easily be used by others.

The energy band diagrams and the density of states for a single layer and two layers of graphene were calculated before in Ref. 9 in which an all-electron density-functional theory calculation within the local density approximation was performed. They concentrated, however, on the dilayer interlayer spacing, and they showed that it differs very little from *AB*-stacked graphite. These calculations could not give any conclusive evidence whether the system of two layers of graphene is a zero-gap semiconductor or a semimetal. The aim of the present paper is to resolve this issue. In contrast to most other approaches we will concentrate on the small energy electronic structure which is the energy range relevant for recent transport experiments.[2–4]

This paper is organized as follows. In Sec. II the details of our tight-binding approach are given. In Sec. III our results are presented and Sec. IV summarizes our conclusions. In the Appendix the relation between our tight-binding parameters and the (experimentally well-known) parameters in the Slonczewski-Weiss-McClure model is obtained.

II. TIGHT-BINDING DESCRIPTION

Figure 1(a) shows schematically the crystal structure of three *AB*-stacked graphene layers. The translational vectors of the crystal structure are

$$\vec{a}_1 = a(\sqrt{3}/2, 1/2, 0), \quad \vec{a}_2 = a(\sqrt{3}/2, -1/2, 0). \tag{1}$$

The in-plane lattice parameter is $a=\sqrt{3}a_0$, with a_0 the nearest-neighbor distance. The corresponding Brillouin zone with the name labels for the high-symmetry points is shown in Fig. 1(b). The reciprocal lattice is given by

$$\vec{b}_1 = \frac{2\pi}{a}(1/\sqrt{3}, 1, 0), \quad \vec{b}_2 = \frac{2\pi}{a}(1/\sqrt{3}, -1, 0). \tag{2}$$

The distance between two layers is c_0. It was shown in Ref. 9 that already for a system of two graphene layers the interplanar spacing and the intraplanar lattice spacing are almost identical to the bulk graphite values. Therefore we use in this work $a_0=1.42$ Å and $c_0=3.35$ Å.

In order to study how the electronic structure changes from a single graphene layer into bulk graphite, we construct a tight-binding Hamiltonian for an arbitrary number of graphene layers. Therefore we extend the original approaches of Refs. 10 and 11 for a single layer to multilayers, with the important addition that starting from two layers of

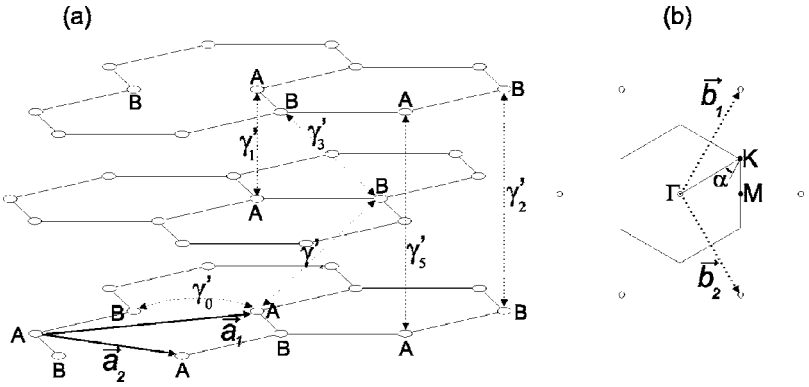

FIG. 1. (a) The crystal structure of three *AB*-stacked graphene layers, together with the correspondence between the tight-binding parameters γ_i' and the interaction between individual carbon atoms. (b) The reciprocal cell of a finite number of graphene layers with the labels for special symmetry points.

graphene, the *A* and *B* type of carbon atoms are inequivalent. In our tight-binding model we limit ourselves to the following interactions between carbon atoms [see also Fig. 1(a)]: the interactions between nearest *A*-*B* carbon atoms in a plane, between nearest *A*-*A*, *A*-*B*, and *B*-*B* carbon atoms between two nearest-neighbor planes, and between nearest *A*-*A* and *B*-*B* carbon atoms between next-nearest-neighbor planes. In previous studies of *AB*-stacked graphite it was shown that the separation between the π bands and the σ bands near the Fermi energy is very large. So it is the π electrons which play the dominant role in the electronic properties of graphite. Therefore, in the following we restrict ourselves to the π bands.

As there are one *A* and one *B* type of carbon atom in each plane *i*, we construct two tight-binding Bloch functions per layer:

$$\psi_{\vec{k}}^{A_i}(\vec{r}) = \frac{1}{\sqrt{N}} \sum_{A_i} \phi_A(\vec{r} - \vec{r}_{A_i}) \exp(i\vec{k} \cdot \vec{r}_{A_i}), \tag{3a}$$

$$\psi_{\vec{k}}^{B_i}(\vec{r}) = \frac{1}{\sqrt{N}} \sum_{B_i} \phi_B(\vec{r} - \vec{r}_{B_i}) \exp(i\vec{k} \cdot \vec{r}_{B_i}). \tag{3b}$$

Here $\vec{r}_{A_i}$ and $\vec{r}_{B_i}$ are the positions of the *A* and *B* carbon atoms in layer *i*, ϕ_A and ϕ_B denote the atomic wave function of an *A* and a *B* carbon atom, and *N* is the number of unit cells. The total eigenfunction for a system of graphene layers is now given by

$$\Psi_{\vec{k}}(\vec{r}) = \sum_{i=1}^{N_l} c_{A_i} \psi_{\vec{k}}^{A_i}(\vec{r}) + \sum_{i=1}^{N_l} c_{B_i} \psi_{\vec{k}}^{B_i}(\vec{r}), \tag{4}$$

with N_l the number of layers. The $2N_l$ coefficients are obtained by diagonalizing the total Hamiltonian for a system of N_l layers on the basis of the tight-binding Bloch functions (3) (we neglect all overlap integrals because of the relatively large separation between the carbon atoms and because we are only interested in the small energy electronic structure around the *K* point). Before developing this tight-binding Hamiltonian we define eight tight-binding parameters (in which *H* is the total Hamiltonian of the system of N_l graphene layers):

$$E_0 + \Delta' = \int \phi_A^*(\vec{r} - \vec{r}_{A_i}) H \phi_A(\vec{r} - \vec{r}_{A_i}) d\vec{r}, \tag{5a}$$

$$E_0 = \int \phi_B^*(\vec{r} - \vec{r}_{B_i}) H \phi_B(\vec{r} - \vec{r}_{B_i}) d\vec{r}, \tag{5b}$$

$$\gamma_0' = \int \phi_A^*(\vec{r} - \vec{r}_{A_i}) H \phi_A(\vec{r} - \vec{r}_{A_i} - \vec{R}_{AB}^j) d\vec{r}, \quad j = 1, \ldots, 3, \tag{5c}$$

$$\gamma_1' = \int \phi_A^*(\vec{r} - \vec{r}_{A_i}) H \phi_A(\vec{r} - \vec{r}_{A_i} \pm \vec{c}_0) d\vec{r}, \tag{5d}$$

$$\gamma_2' = \int \phi_B^*(\vec{r} - \vec{r}_{B_i}) H \phi_B(\vec{r} - \vec{r}_{B_i} \pm 2\vec{c}_0) d\vec{r}, \tag{5e}$$

$$\gamma_3' = \int \phi_B^*(\vec{r} - \vec{r}_{B_i}) H \phi_B(\vec{r} - \vec{r}_{B_i} + \vec{R}_{AB}^j \pm \vec{c}_0) d\vec{r}, \quad j = 1, \ldots, 3, \tag{5f}$$

$$\gamma_4' = \int \phi_A^*(\vec{r} - \vec{r}_{A_i}) H \phi_A(\vec{r} - \vec{r}_{B_i} + \vec{R}_{AB}^j \pm \vec{c}_0) d\vec{r}, \quad j = 1, \ldots, 3, \tag{5g}$$

$$\gamma_5' = \int \phi_A^*(\vec{r} - \vec{r}_{A_i}) H \phi_A(\vec{r} - \vec{r}_{A_i} \pm \vec{c}_0) d\vec{r}, \tag{5h}$$

with

$$\vec{R}_{AB}^1 = a(1/\sqrt{3}, 0, 0), \quad \vec{R}_{AB}^2 = a(-1/2\sqrt{3}, 1/2, 0),$$

$$\vec{R}_{AB}^3 = a(-1/2\sqrt{3}, -1/2, 0). \tag{6}$$

Δ' is the difference in crystal field experienced by the inequivalent carbon atoms *A* and *B*.

The tight-binding Hamiltonian for a general number of graphene layers can be obtained if one knows the following matrix elements:

$$\langle \psi_{\vec{k}}^{A_i} | H | \psi_{\vec{k}}^{A_i} \rangle \approx \frac{1}{N} \sum_{A_i} \int \phi_A^*(\vec{r} - \vec{r}_{A_i}) H \phi_A(\vec{r} - \vec{r}_{A_i}) d\vec{r} = E_0 + \Delta', \tag{7a}$$

$$\langle \psi_{\vec{k}}^{A_i}|H|\psi_{\vec{k}}^{B_i}\rangle \approx \frac{1}{N}\sum_{A_i}\int \phi_A^*(\vec{r}-\vec{r}_{A_i}) \times H\left(\sum_{j=1}^{3} e^{(-1)^{i+1}i\vec{k}\cdot\vec{R}_{AB}^j}\phi_B(\vec{r}-\vec{r}_{A_i}-\vec{R}_{AB}^j)\right)d\vec{r} = \gamma_0' f(k_x,k_y) \text{ if } i \text{ is odd and } \gamma_0' f^*(k_x,k_y) \text{ if } i \text{ is even}, \tag{7b}$$

$$\langle \psi_{\vec{k}}^{A_i}|H|\psi_{\vec{k}}^{A_{i+1}}\rangle \approx \frac{1}{N}\sum_{A_i}\int \phi_A^*(\vec{r}-\vec{r}_{A_i})H\phi_A(\vec{r}-\vec{r}_{A_i}-\vec{c}_0) = \gamma_1', \tag{7c}$$

$$\langle \psi_{\vec{k}}^{A_i}|H|\psi_{\vec{k}}^{B_{i+1}}\rangle \approx \frac{1}{N}\sum_{A_i}\int \phi_A^*(\vec{r}-\vec{r}_{A_i}) \times H\left(\sum_{j=1}^{3} e^{(-1)^{i}i\vec{k}\cdot\vec{R}_{AB}^j}\phi_B(\vec{r}-\vec{r}_{A_i}+\vec{R}_{AB}^j-\vec{c}_0)\right)d\vec{r} = \gamma_4' f^*(k_x,k_y) \text{ if } i \text{ is odd and } \gamma_4' f(k_x,k_y) \text{ if } i \text{ is even}, \tag{7d}$$

$$\langle \psi_{\vec{k}}^{A_i}|H|\psi_{\vec{k}}^{A_{i+2}}\rangle \approx \frac{1}{N}\sum_{A_i}\int \phi_A^*(\vec{r}-\vec{r}_{A_i})H\phi_A(\vec{r}-\vec{r}_{A_i}-2\vec{c}_0)d\vec{r} = \gamma_5', \tag{7e}$$

$$\langle \psi_{\vec{k}}^{B_i}|H|\psi_{\vec{k}}^{B_i}\rangle \approx \frac{1}{N}\sum_{B_i}\int \phi_B^*(\vec{r}-\vec{r}_{B_i})H\phi_B(\vec{r}-\vec{r}_{B_i})d\vec{r} = E_0, \tag{7f}$$

$$\langle \psi_{\vec{k}}^{B_i}|H|\psi_{\vec{k}}^{A_{i+1}}\rangle = \langle \psi_{\vec{k}}^{A_i}|H|\psi_{\vec{k}}^{B_{i+1}}\rangle, \tag{7g}$$

$$\langle \psi_{\vec{k}}^{B_i}|H|\psi_{\vec{k}}^{B_{i+1}}\rangle \approx \sum_{B_i}\int \phi_B^*(\vec{r}-\vec{r}_{B_i}) \times H\left(\sum_{j=1}^{3} e^{(-1)^{i+1}i\vec{k}\cdot\vec{R}_{AB}^j}\phi_B(\vec{r}-\vec{r}_{B_i}-\vec{R}_{AB}^j-\vec{c}_0)\right)d\vec{r} = \gamma_3' f(k_x,k_y) \text{ if } i \text{ is odd and } \gamma_3' f^*(k_x,k_y) \text{ if } i \text{ is even}, \tag{7h}$$

$$\langle \psi_{\vec{k}}^{B_i}|H|\psi_{\vec{k}}^{B_{i+2}}\rangle \approx \frac{1}{N}\sum_{B_i}\int \phi_B^*(\vec{r}-\vec{r}_{B_i})H\phi_B(\vec{r}-\vec{r}_{B_i}-2\vec{c}_0)d\vec{r} = \gamma_2'. \tag{7i}$$

The function $f(k_x,k_y)$ is given by

$$f(k_x,k_y) = e^{ik_x a/\sqrt{3}} + 2e^{-ik_x a/2\sqrt{3}}\cos(k_y a/2). \tag{8}$$

With these expressions one can construct the tight-binding Hamiltonian for an arbitrary number of layers, N_l:

$$\begin{pmatrix} \langle \psi_{\vec{k}}^{A_1}|H|\psi_{\vec{k}}^{A_1}\rangle & \langle \psi_{\vec{k}}^{A_1}|H|\psi_{\vec{k}}^{B_1}\rangle & \cdots & \langle \psi_{\vec{k}}^{A_1}|H|\psi_{\vec{k}}^{B_{N_l}}\rangle \\ \langle \psi_{\vec{k}}^{B_1}|H|\psi_{\vec{k}}^{A_1}\rangle & \langle \psi_{\vec{k}}^{B_1}|H|\psi_{\vec{k}}^{B_1}\rangle & \cdots & \langle \psi_{\vec{k}}^{B_1}|H|\psi_{\vec{k}}^{B_{N_l}}\rangle \\ \langle \psi_{\vec{k}}^{A_2}|H|\psi_{\vec{k}}^{A_1}\rangle & \langle \psi_{\vec{k}}^{A_2}|H|\psi_{\vec{k}}^{B_1}\rangle & \cdots & \langle \psi_{\vec{k}}^{A_2}|H|\psi_{\vec{k}}^{B_{N_l}}\rangle \\ \vdots & \vdots & \ddots & \vdots \\ \langle \psi_{\vec{k}}^{B_{N_l}}|H|\psi_{\vec{k}}^{A_1}\rangle & \langle \psi_{\vec{k}}^{B_{N_l}}|H|\psi_{\vec{k}}^{B_1}\rangle & \cdots & \langle \psi_{\vec{k}}^{B_{N_l}}|H|\psi_{\vec{k}}^{B_{N_l}}\rangle \end{pmatrix}. \tag{9}$$

The values for the eight tight-binding parameters are obtained by comparing the tight-binding model for bulk graphite with the Slonczewski-Weiss-McClure (SWMcC) model[12,13] as shown in the Appendix. The correspondence and the values used (taken from Ref. 1) are given in Table I. Note that the values are given for one, two, and more than two layers, because not all parameters are meaningful for the system of just one or two layers. The values for E_0 and Δ' for $N_l=2$ are chosen to be equal to the ones for $N_l=3$ which follow from a comparison with the SWMcC model.

TABLE I. The relation between the parameters from the tight-binding (TB) model and the SWMcC model, together with the values of the used tight-binding parameters for $N_l=1$, $N_l=2$, and $N_l>2$, expressed in eV, taken from Ref. 1.

TB parameter	SWMcC parameter	Value for $N_l=1$	Value for $N_l=2$	Value for $N_l>2$
E_0	γ_2	0	−0.0206	−0.0206
Δ'	$\Delta-\gamma_2+\gamma_5$	0	0.0366	0.0366
γ_0'	γ_0	3.12	3.12	3.12
γ_1'	γ_1		0.377	0.377
γ_2'	$\gamma_2/2$			−0.0103
γ_3'	γ_3		0.29	0.29
γ_4'	$-\gamma_4$		−0.120	−0.120
γ_5'	$\gamma_5/2$			0.0125

III. RESULTS

In Sec. III A we make a comparison between a single graphene layer and a system consisting of two graphene layers. Multilayers with more than two graphene layers are considered in Sec. III B.

A. Systems consisting of one and two graphene layers

First we compare the energy band diagram of a single graphene layer with the one of two graphene layers. The energy bands for the single graphene layer along the $M\Gamma KM$ lines in the Brillouin zone are shown in Fig. 2. The Fermi energy is located at $E=0$ where the two bands cross at the K point, leading to the fact that a single graphene layer is a

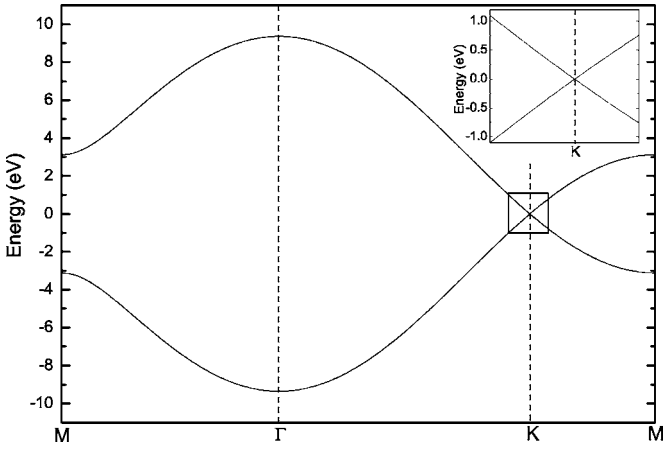

FIG. 2. The band structure of a single graphene layer along $M\Gamma KM$. The inset is an enlargement of the region indicated by the square around the K point.

zero-gap semiconductor. Around the K point the spectrum is linear as shown in the inset and it is given by $E=\pm\frac{\sqrt{3}}{2}\gamma_0'\kappa$, until first order in κ which is the distance from the K point. If one compares this expression with the relativistic energy expression $E=(m^2c^4+p^2c^2)^{1/2}$, one can see that the dispersion relation of a single graphene layer mimics a system of relativistic (Dirac) particles with zero rest mass and an effective speed of light $c=\sqrt{3}\gamma_0'a/2\hbar\approx 1.01\times 10^6$ m/s, which is almost 300 times smaller than the speed of light in vacuum.

The corresponding energy band diagram for the system of two graphene layers is shown in Fig. 3, together with a close-up of the spectrum around the K point and around $E=0$. Notice that the number of levels is doubled. The spectrum is clearly no longer linear around the K point, but parabolic. If one moves away from the K point, the spectrum becomes again linear. At first sight one would conclude that the bands just touch at the K point. However, a more detailed investigation presented in Fig. 4 shows a small overlap and an interaction leading to anticrossings between the conduction and valence bands. Figure 4(a) shows an enlargement of the bands around $E=0$ from the K point in the direction of

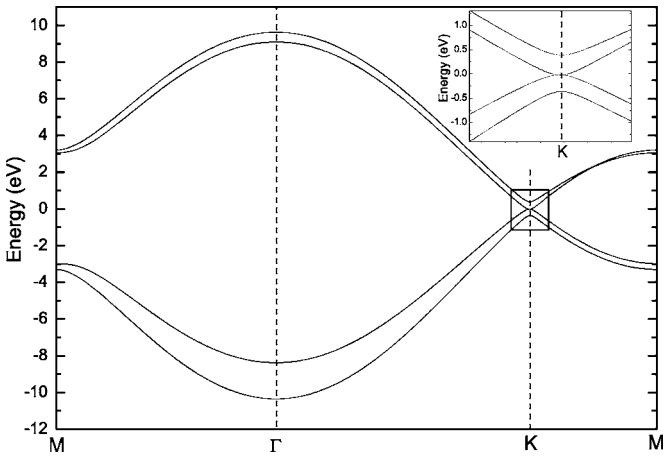

FIG. 3. The band structure of two graphene layers along $M\Gamma KM$. The square region is enlarged in the inset.

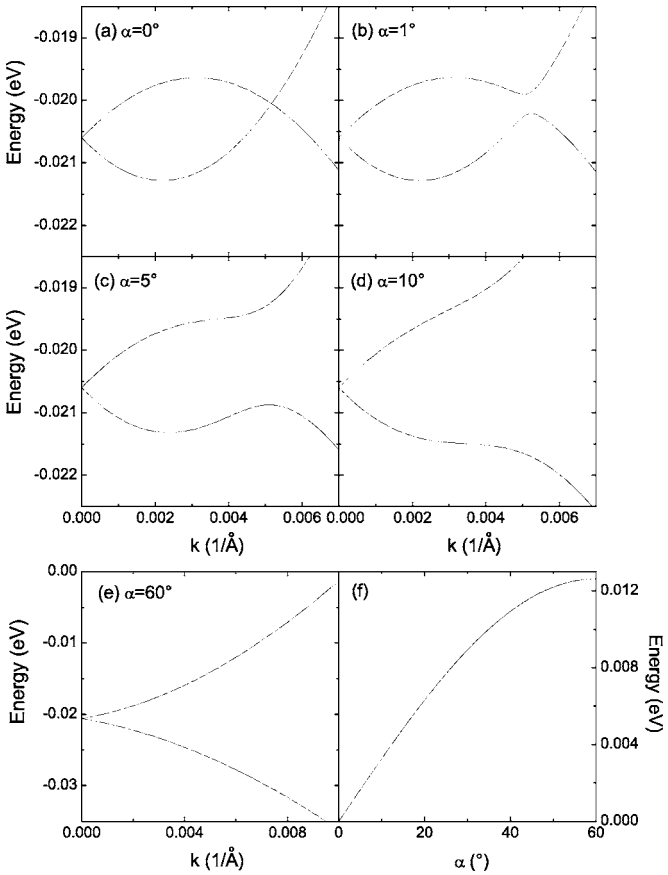

FIG. 4. The band structure of two graphene layers close to the K point along a line which makes an angle α with the ΓK line [see Fig. 1(b)], for (a) $\alpha=0°$ (i.e., from the K point in the direction of the Γ point), (b) $\alpha=1°$, (c) $\alpha=5°$, (d) $\alpha=10°$, and (e) $\alpha=60°$ (i.e., from the K point in the direction of the M point). (f) The band gap as function of the angle α at $k=0.0052$ Å^{-1}.

the Γ point. There is clearly a small band overlap between the conduction and the valence band of only 1.6 meV. This small band overlap is caused by the interaction between B and B' carbon atoms, and it disappears if one puts $\gamma_3'=0$. This overlap is also present in bulk graphite and was discussed shortly in the original paper of Slonczewski and Weiss (see Fig. 8 in Ref. 12). Figure 4 shows further how the crossing of the bands changes into an anticrossing if one considers a line through the K point which makes an angle α with the Γ-K line [as defined in Fig. 1(b)]. For $\alpha=0$ and $\alpha=\pi/3$, the bands can be well fitted by the expression $E=a\pm\sqrt{m^2c^4+(p-p_0)^2c^2}$ with, respectively, $a=-0.174$ eV, $m=2.4\times 10^{-32}$ kg$=0.026m_e$, $p_0=0.0022$ m$^{-1}\times\hbar$, and $a=0.2075$ eV, $m=3.57\times 10^{-32}$ kg$=0.039m_e$, $p_0=0.0031$ m$^{-1}\times\hbar$ for $\alpha=0$, and $a=-0.163$ eV, $m=2.23\times 10^{-32}$ kg $=0.024m_e$, $p_0=-0.0015$ m$^{-1}\times\hbar$, and $a=0.203$ eV, $m=3.5\times 10^{-32}$ kg$=0.038m_e$, $p_0=-0.0032$ m$^{-1}\times\hbar$ for $\alpha=\pi/3$. $c=\sqrt{3}\gamma_0'a/2\hbar\approx 1.01\times 10^6$ m/s was taken the same as for a single layer. Notice that the crossing at $k=0.0052$ Å^{-1} results in an anticrossing: Figure 4(f) shows the band gap in this k point as a function of α. We found that this splitting is well described by $0.0126\sin(3\alpha/2)$ eV. Clearly, the system consisting of two graphene layers is a semimetal, but with a very

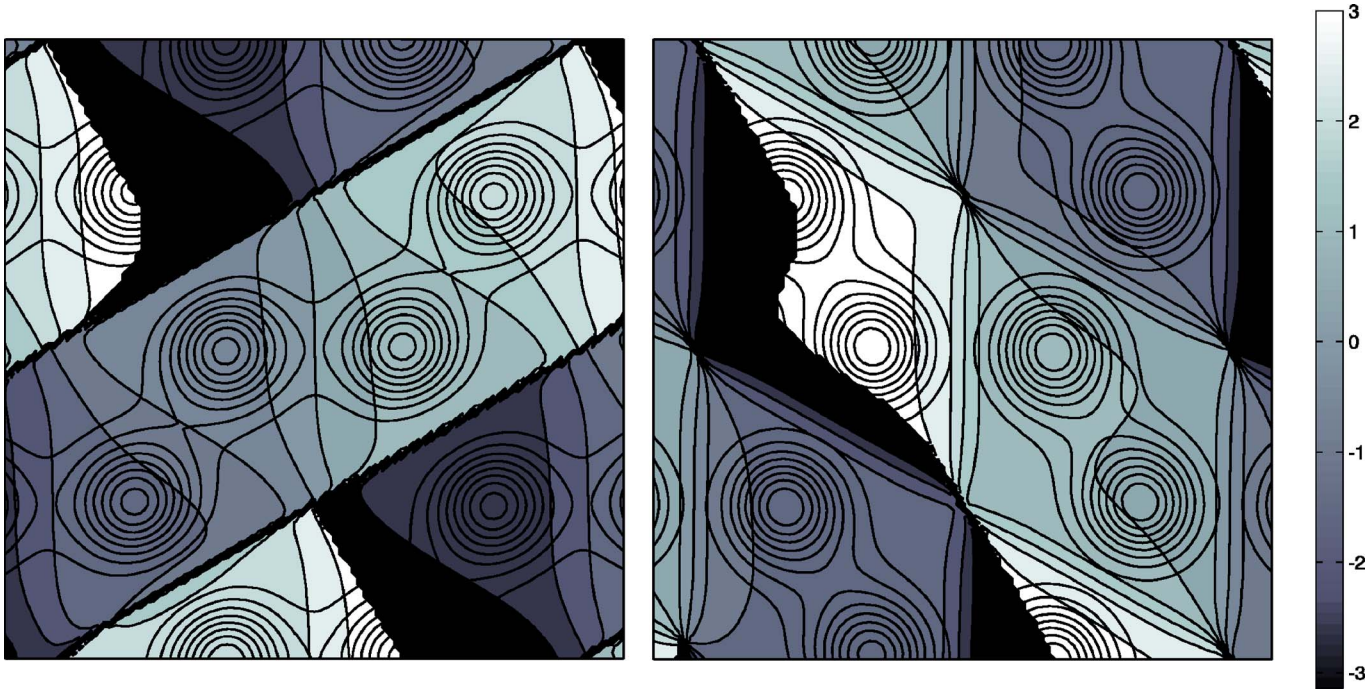

FIG. 5. (Color online) The phase (using gray coloring with the corresponding scale at the right) of the two degenerate wave functions at the K point for a single graphene layer, with a contourplot of the electron density superimposed.

small band overlap and with a crossing of the conduction and valence bands only along one direction in the Brillouin zone.

Approximate expressions for the energy levels close to the Fermi energy around the K point can be obtained by expanding the Hamiltonian of Eq. (9) until first order in k space, by neglecting the energy splitting between inequivalent A and B atoms and by neglecting the smallest coupling parameter γ_4. They are

$$E = \pm \frac{1}{2\sqrt{2}}\{4\gamma_1^2 + 3a^2(2\gamma_0^2 + \gamma_3^2)(\kappa_x^2 + \kappa_y^2) - [16\gamma_1^4 + 48\sqrt{3}a^3\gamma_0^2\gamma_1\gamma_3\kappa_y(-3\kappa_x^2 + \kappa_y^2) + 24a^2\gamma_1^2(2\gamma_0^2 - \gamma_3^2)(\kappa_x^2 + \kappa_y^2) + 9a^4\gamma_3^2(4\gamma_0^2 + \gamma_3^2)(\kappa_x^2 + \kappa_y^2)^2]^{1/2}\}^{1/2}, \quad (10)$$

with (κ_x, κ_y) the wave vector measured from the K point. In this approximation the crossing occurs at $k=0.0053$ Å^{-1} and the splitting is given by $0.0129 \sin(3\alpha/2)$ eV. This expression agrees with the one in Ref. 7 when a possible influence of the environment is neglected. Within this approximation two layers of graphene is still a semimetal with the same band overlap of 1.6 meV.

Another remarkable difference between a single layer and two layers of graphene is found if one considers the wave function at the K point. To obtain a qualitative description of the wave function we have chosen the atomic orbital $\phi_A(\vec{r})$ and $\phi_B(\vec{r})$ as the p_z wave function for hydrogenlike atoms:

$$\phi(\vec{r}) = \frac{1}{4\sqrt{2\pi}}(Z/a_B)^{3/2}(Zr/a_B)\exp(-Zr/2a_B)\cos\theta,$$

with $Z=6$ and a_B the Bohr radius. In Figs. 5 and 6 we show cuts through the wave functions at 1 Å above a graphene layer. Figure 5 is the result for a single graphene layer. It shows the phase of the wave functions of the two degenerate levels at the K point with the density superimposed on top of it. The hexagonal structure of the graphene layer is clearly seen. The results for the system of two layers of graphene are shown in Fig. 6. Again the phase of the wave functions of the two degenerate levels at the K point are shown, together with the density. The difference with a single graphene layer is remarkable. The density in Fig. 6 only comes from B and B' carbon atoms; the factors in front of $\psi_{\vec{k}}^{A1}(\vec{r})$ and $\psi_{\vec{k}}^{A2}(\vec{r})$ are zero. From this comparison we can conclude that for a single graphene layer all electrons in the p_z orbital contribute to the transport properties, while for the system with two graphene layers the main contribution to transport comes from the p_z electrons located around the B- and B'-type carbon atoms. Also note that for the system consisting of two graphene layers vortices are present—i.e., zeros in the wave function around which the phase changes by 2π—and these vortices are arranged in a hexagonal lattice.

B. More than two graphene layers

In order to investigate how the electronic structure evolves to bulk graphite with increasing number of graphene layers, we first discuss the band structure of graphite. The relevant region for electronic transport is the region around the Fermi energy and in particular along the HKH band edge. Figure 7 shows the band diagram in this region as obtained by diagonalizing Hamiltonian (A8). Along the HKH band edge there are three energy bands E_1, E_2, and E_3, of which E_3 is twofold degenerate. The twofold-degenerate energy band leads to a band overlap of $2\gamma_2 \approx 41$ meV which makes bulk

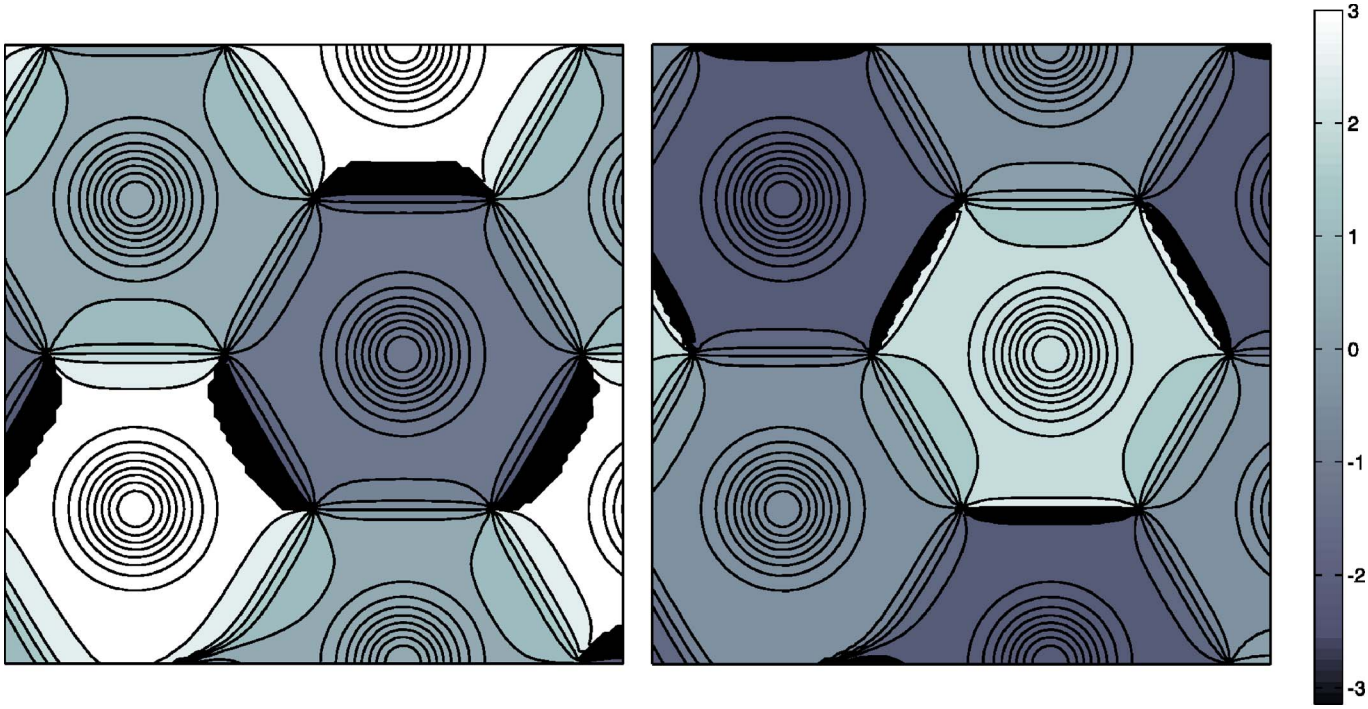

FIG. 6. (Color online) The same as Fig. 5 but now for two layers of graphene.

graphite a semimetal. This band overlap, which is 25 times larger than the overlap for two graphene layers, is caused by the interaction between the B carbon atoms of next-nearest-neighbor planes. The Fermi surface consists of electron and hole pockets. Because $\gamma_2 < 0$, the electron pocket is situated around the K point, while the hole pockets are situated around the H points. The splitting of the energy levels at the H point equals Δ (which is related to the crystal field splitting between inequivalent A and B carbon atoms). Because the Fermi energy $E_F > |\Delta|$, the hole pocket protrudes beyond the H point, leading to a minority hole surface.

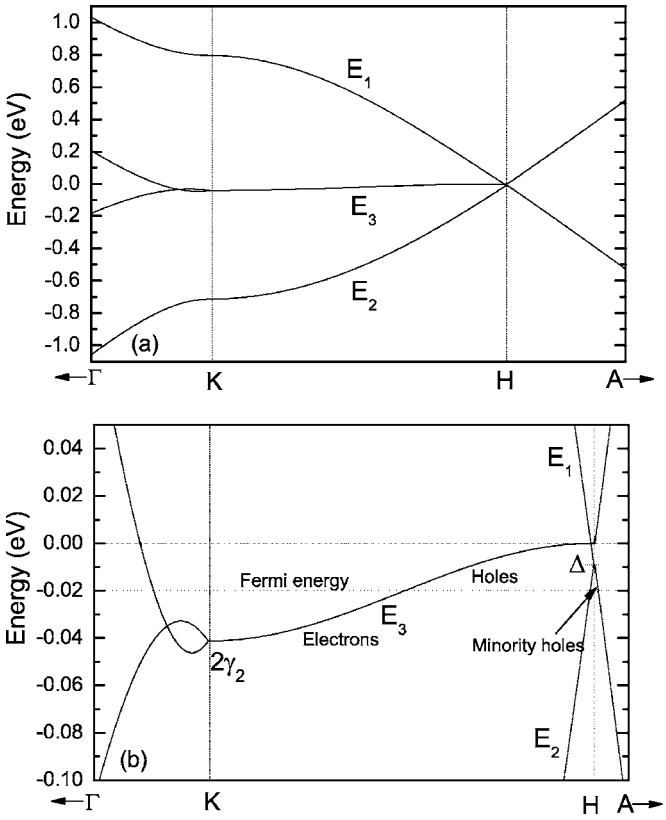

FIG. 7. (a) The band diagram of bulk graphite around the HKH band edge. (b) Close-up of (a) around the Fermi energy.

Let us now consider a system consisting of three graphene layers. The band diagram together with a close-up around the K point is shown in Figs. 8(a) and 8(b), respectively. At the K point around zero energy several bands cross while other bands show anticrossings. It is clear that the band structure around the K point becomes more and more complex with increasing number of graphene layers: the number of layers around the Fermi energy at the K point is doubled in comparison to systems with one and two graphene layers. In contrast to the double-layer system, crossings do not become anticrossings if one considers a line through the K point which makes an angle α with the Γ-K line. The band diagram can be understood as a combination of the band diagram of a single graphene layer (Fig. 2) and the band diagram of the system consisting of two graphene layers (Fig. 3). The four bands around the Fermi energy at the K point are labeled by A, B, C, and D in Fig. 8(b). While bands B and C remind us of the two bands of the two-layer system, but now with anticrossings, bands A and D show an almost linear dispersion and mimic the bands of a single graphene layer with the additional opening of a gap at the K point of 13.8 meV. Bands A and D are almost independent of the angle α [as defined in Fig. 1(b)], in contrast to bands B and C.

In order to see how the energy levels at the K point for a finite number of layers evolve into the band structure of graphite along the HKH edge (see Fig. 11, below), we show

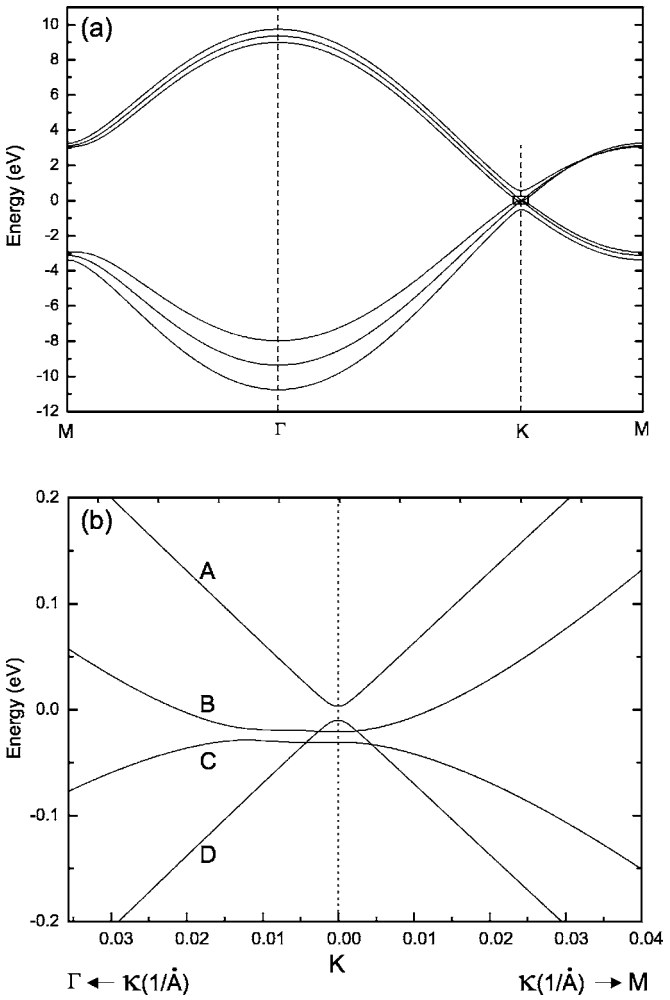

FIG. 8. (a) The band structure of three graphene layers along $M\Gamma KM$. (b) Enlargement of the region around the K point as indicated by the little box in (a).

in Figs. 9(a)–9(e) a plot of the energy levels at the K point, in increasing order and equally distributed over the interval $[0, \pi/2c_0]$ for three up to seven levels. In Fig. 9(f) the plot is shown for 20 graphene layers. The start and end of the curves evolve clearly into the levels marked E_1 and E_2 in Fig. 7 for bulk graphite, while it is clear that in between the doubly degenerate level E_3 is built up. It consists of N_l energy levels if N_l is even and N_l+1 if N_l is odd. This also allows us to make an estimate for the band overlap in the finite layer systems—i.e., the difference in energy between the last and first level which build up level E_3. This is shown in Fig. 10, where the solid horizontal line is the result for bulk graphite. It is clear that all systems with $N_l \geqslant 3$ are semimetals. For 11 or more layers, the difference with the bulk band overlap is smaller than 10%.

Finally we want to remark that the result for the wave functions at the K point for the system consisting of three and more graphene layers is similar to that for two graphene layers: the levels that eventually evolve into the E_3 level consist only of B-type carbon atoms (except for the highest levels close to the E_1 level which can consist only of A- type carbon atoms). The fact that only the B atoms build up the electron density at the K point for the levels close at the Fermi energy is also the case for bulk AB-stacked graphite: along the whole HKH edge of the Brillouin zone only the B and B' carbon atoms contribute to the two degenerate E_3 levels.

IV. CONCLUSIONS

We investigated the electronic structure of a finite number of graphene layers around the K point and compared it with bulk graphite. We used a tight-binding approach similar to the Slonczewski-Weiss-McClure model for bulk graphite. A single layer of graphene is a zero-gap semiconductor which shows a linear photonlike spectrum around the Fermi energy at the K point. The system consisting of two layers of graphene, however, shows an almost parabolic spectrum around the Fermi energy at the K point. A close-up of the energy bands of two layers of graphene shows a small band overlap close to the K point in the direction of the Γ point. This overlap is due to the interaction between the B and B' carbon atoms of the two layers and amounts only to 1.6 meV. The crossing between the two overlapping bands transforms into an anticrossing when one moves away from the ΓK line. The system of two graphene layers is thus a semimetal, but with a very small overlap and with a crossing of the bands only along one direction in the Brillouin zone. Starting from three graphene layers on, multilayer graphene systems are all semimetals in which the semimetallic behavior is caused by the interaction between the B carbon atoms of next-nearest-neighbor planes. In general, the band overlap increases with increasing number of layers. From 11 layers on the difference with the band overlap in bulk graphite ($\approx$41 meV) is less than 10%. There is also a remarkable difference in the wave functions at the K point for the levels around the Fermi energy between a single graphene layer and systems consisting of more graphene layers.

ACKNOWLEDGMENTS

This work is supported by the Flemish Science Foundation (FWO-VI) and the "Belgian Science Policy." We thank A. Geim for interesting correspondence.

APPENDIX: RELATION BETWEEN SWMcC PARAMETERS AND THE TIGHT-BINDING PARAMETERS

The SWMcC model gives a phenomenological treatment of the electronic structure of graphite based on crystal symmetry. The model presents the most general form for the Hamiltonian that is consistent with the crystal symmetry and is valid in the vicinity of the Brillouin zone edges (the Brillouin zone of bulk graphite is shown in Fig. 11 together with the labels for special symmetry points). In the k_z direction a Fourier expansion is made and rapid convergence is obtained (which is the ideal tight-binding situation) because of the weak interplanar binding. In the plane, a $\vec{k}\cdot\vec{p}$ expansion is made. The SWMcC model is commonly written in terms of the 4×4 Hamiltonian for the π bands:

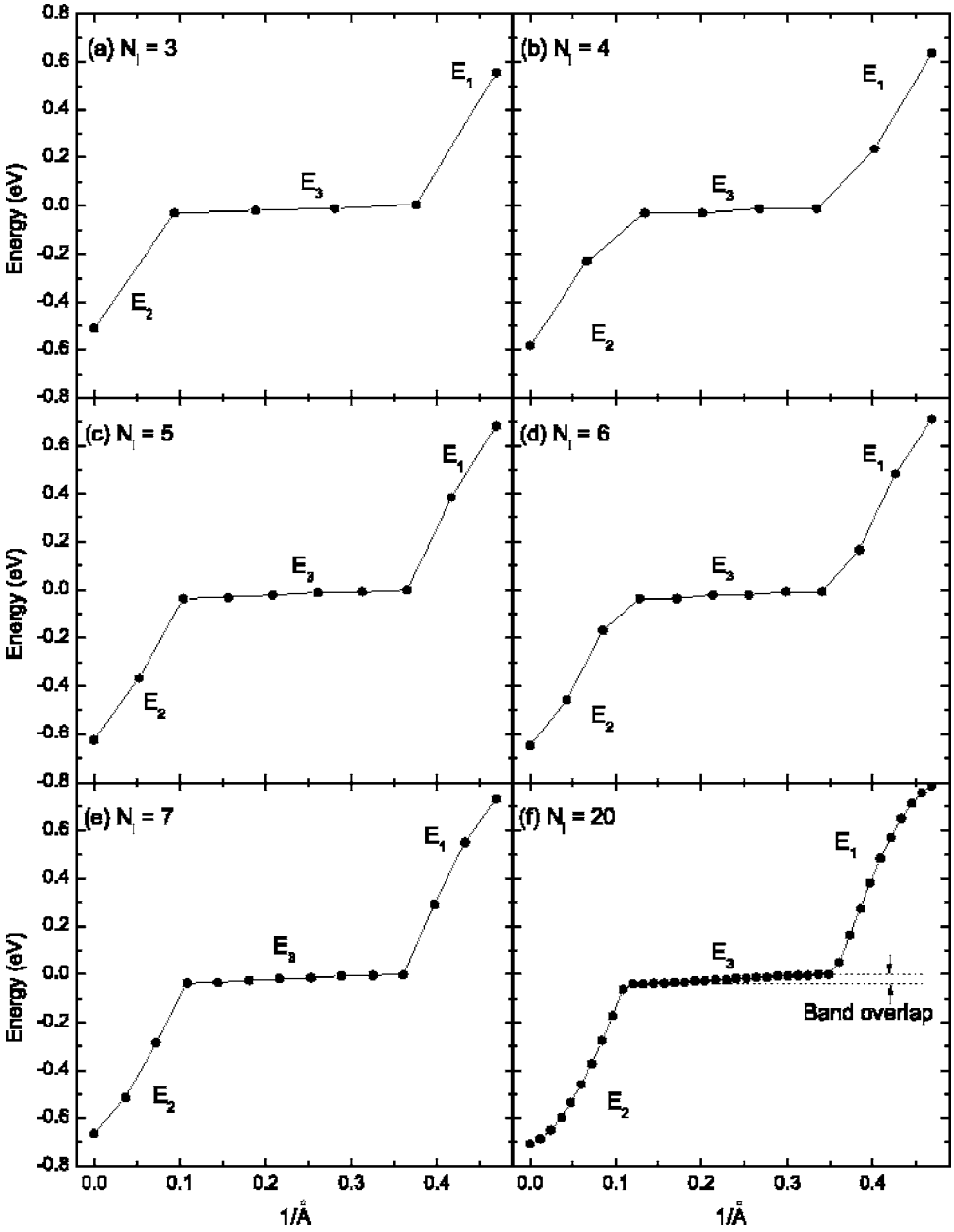

FIG. 9. The sorted energy levels of (a) 3, (b) 4, (c) 5, (d) 6, (e) 7, and (f) 20 graphene layers at the K point, plotted equidistantly over the interval $[0, \pi/2c_0]$.

$$H = \begin{pmatrix} E_1 & 0 & H_{13} & H_{13}^* \\ 0 & E_2 & H_{23} & -H_{23}^* \\ H_{13}^* & H_{23}^* & E_3 & H_{33} \\ H_{13} & -H_{23} & H_{33}^* & E_3 \end{pmatrix}, \tag{A1}$$

where the band edge energies are given by

$$E_1 = \Delta + \gamma_1\Gamma + \frac{1}{2}\gamma_5\Gamma^2, \tag{A2}$$

$$E_2 = \Delta - \gamma_1\Gamma + \frac{1}{2}\gamma_5\Gamma^2, \tag{A3}$$

$$E_3 = \frac{1}{2}\gamma_2\Gamma^2, \tag{A4}$$

and the coupling terms are

$$H_{13} = (-\gamma_0 + \gamma_4\Gamma)\sigma\exp(i\alpha)/\sqrt{2}, \tag{A5}$$

$$H_{23} = (\gamma_0 + \gamma_4\Gamma)\sigma\exp(i\alpha)/\sqrt{2}, \tag{A6}$$

$$H_{33} = \gamma_3\Gamma\sigma\exp(i\alpha), \tag{A7}$$

in which α is the angle between $\vec{k}$ and the ΓK direction, $\Gamma = 2\cos(k_z c/2)$, $\sigma = \sqrt{3}a\kappa/2$, and κ is the in-plane wave vector measured from the Brillouin zone edges. In order to find the relation between the SWMcC parameters and the parameters

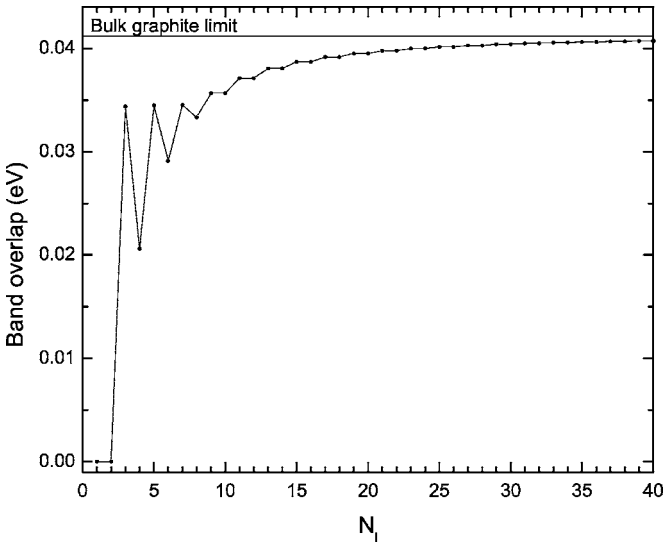

FIG. 10. The energy difference between the last and first energy levels at the K point which build up the E_3 energy band of graphite for N_l graphene layers. The solid horizontal curve is the limiting value for bulk graphite.

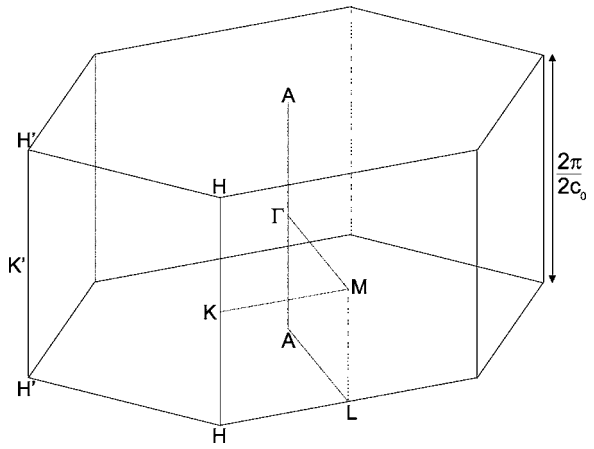

FIG. 11. The Brillouin zone of bulk graphite together with the labels for special symmetry points.

of our tight-binding model we first construct the tight-binding Hamiltonian for graphite using the definitions of Eqs. (5) and (8):

$$\begin{pmatrix} E_0+\Delta'+\gamma_5'(\Gamma^2-2) & \gamma_0' f(k_x,k_y) & \gamma_1'\Gamma & \gamma_4'\Gamma f^*(k_x,k_y) \\ \gamma_0' f^*(k_x,k_y) & E_0+\gamma_2'(\Gamma^2-2) & \gamma_4'\Gamma f^*(k_x,k_y) & \gamma_3\Gamma f(k_x,k_y) \\ \gamma_1'\Gamma & \gamma_4\Gamma f(k_x,k_y) & E_0+\Delta'+\gamma_5'(\Gamma^2-2) & \gamma_0 f^*(k_x,k_y) \\ \gamma_4'\Gamma f(k_x,k_y) & \gamma_3'\Gamma f^*(k_x,k_y) & \gamma_0' f(k_x,k_y) & E_0+\gamma_2'(\Gamma^2-2) \end{pmatrix}. \tag{A8}$$

In order to obtain the relation between the SWMcC model (which are known from experiments) and the parameters of the tight-binding model we consider special points and lines in the Brillouin zone for which it is easy to calculate the eigenenergies in both models. Furthermore, each of the six parameters γ_i is proportional to the parameter γ_i' defined in Sec. II as they are both related to the same interaction between two atoms in the graphite lattice as shown in Fig. 1.

Along the HKH line we have $k_x=2\pi/\sqrt{3}a, k_y=2\pi/3a$, and thus $f=0$. Along the HKH line the tight-binding hamiltonian is given by

$$\begin{pmatrix} E_0+\Delta'+\gamma_5'(\Gamma^2-2) & 0 & \gamma_1'\Gamma & 0 \\ 0 & E_0+\gamma_2'(\Gamma^2-2) & 0 & 0 \\ \gamma_1'\Gamma & 0 & E_0+\Delta'+\gamma_5'(\Gamma^2-2) & 0 \\ 0 & 0 & 0 & E_0+\gamma_2'(\Gamma^2-2) \end{pmatrix}, \tag{A9}$$

with the corresponding eigenenergies

$$E_{1,2}=E_0+\Delta'-2\gamma_5'\pm\gamma_1'\Gamma+\gamma_5'\Gamma^2, \tag{A10}$$

$$E_3=E_0-2\gamma_2'+\gamma_2'\Gamma^2. \tag{A11}$$

They must be compared with the energies at the Brillouin zone edge obtained by the SWMcC model:

$$E_{1,2}=\Delta\pm\gamma_1\Gamma+\frac{1}{2}\gamma_5\Gamma^2, \tag{A12}$$

$$E_3=\frac{1}{2}\gamma_2\Gamma^2. \tag{A13}$$

Equating both results yields

$$E_0=2\gamma_2', \tag{A14}$$

$$\gamma_1'=\gamma_1, \tag{A15}$$

$$\gamma_2'=\gamma_2/2, \tag{A16}$$

$$\gamma_5' = \gamma_5/2, \tag{A17}$$

$$\Delta' = \Delta - \gamma_2 + \gamma_5. \tag{A18}$$

This still leaves γ_0', γ_3', and γ_4' to be determined.

Let us now calculate the energies along the ΓK line until first order in κ. Along this line we have

$$k_x = \frac{\sqrt{3}}{2}\left(\frac{4\pi}{3a} - \kappa\right), \tag{A19}$$

$$k_y = \frac{1}{2}\left(\frac{4\pi}{3a} - \kappa\right). \tag{A20}$$

This gives, for $f(k_x, k_y)$ until first order in κ,

$$f(k_x, k_y) = f(\kappa) \approx \frac{\sqrt{3}}{2}\kappa a = \sigma. \tag{A21}$$

The tight-binding Hamiltonian along the ΓK line becomes (with also $\Gamma = 2$)

$$\begin{pmatrix} E_0 + \Delta' + 2\gamma_5' & \gamma_0'\sigma & 2\gamma_1' & 2\gamma_4'\sigma \\ \gamma_0'\sigma & E' + 2\gamma_2' & 2\gamma_4'\sigma & 2\gamma_3'\sigma \\ 2\gamma_1' & 2\gamma_4'\sigma & E_0 + \Delta' + 2\gamma_5' & \gamma_0'\sigma \\ 2\gamma_4'\sigma & 2\gamma_3'\sigma & \gamma_0'\sigma & E_0 + 2\gamma_2' \end{pmatrix}, \tag{A22}$$

with the corresponding eigenenergies

$$E_{1,2} = E_0 + \frac{\Delta'}{2} + \gamma_5' + \gamma_2' + \gamma_3'\sigma + \gamma_1' \pm \frac{1}{2}\sqrt{C + D}, \tag{A23}$$

$$E_{3,4} = E_0 + \frac{\Delta'}{2} + \gamma_5' + \gamma_2' - \gamma_3'\sigma - \gamma_1' \pm \frac{1}{2}\sqrt{C - D}, \tag{A24}$$

with

$$C = \Delta'^2 + 4\Delta'\gamma_5' + 4\gamma_0'^2\sigma^2 + 4\gamma_3'^2\sigma^2 - 4\gamma_2'\Delta' - 8\gamma_2'\gamma_5' - 8\gamma_3'\sigma\gamma_1' + 4\gamma_1'^2 + 16\gamma_4'^2\sigma^2 + 4\gamma_2'^2, \tag{A25}$$

$$D = 16\gamma_0'\sigma^2\gamma_4' + 4\gamma_1'\Delta' + 8\gamma_1'\gamma_5' - 8\sigma\gamma_5'\gamma_3' - 8\gamma_2'\gamma_1' + 8\gamma_3'\gamma_2'\sigma - 4\Delta'\gamma_3\sigma. \tag{A26}$$

The SWMcC Hamiltonian along the ΓK line is

$$\begin{pmatrix} \Delta + 2\gamma_1 + 2\gamma_5 & 0 & (-\gamma_0 + 2\gamma_4)\sigma/\sqrt{2} & (-\gamma_0 + 2\gamma_4)\sigma/\sqrt{2} \\ 0 & \Delta - 2\gamma_1 + 2\gamma_5 & (\gamma_0 + 2\gamma_4)\sigma/\sqrt{2} & -(\gamma_0 + 2\gamma_4)\sigma/\sqrt{2} \\ (-\gamma_0 + 2\gamma_4)\sigma/\sqrt{2} & (\gamma_0 + 2\gamma_4)\sigma/\sqrt{2} & 2\gamma_2 & 2\gamma_3\sigma \\ (-\gamma_0 + 2\gamma_4)\sigma/\sqrt{2} & -(\gamma_0 + 2\gamma_4)\sigma/\sqrt{2} & 2\gamma_3\sigma & 2\gamma_2 \end{pmatrix}, \tag{A27}$$

with corresponding eigenenergies

$$E_{1,2} = \frac{\Delta}{2} + \gamma_5 + \gamma_2 + \gamma_3\sigma + \gamma_1 \pm \frac{1}{2}\sqrt{C + D}, \tag{A28}$$

$$E_{3,4} = \frac{\Delta}{2} + \gamma_5 + \gamma_2 - \gamma_3\sigma - \gamma_1 \pm \frac{1}{2}\sqrt{C - D}, \tag{A29}$$

with

$$C = \Delta^2 + 4\Delta\gamma_5 + 4\gamma_5^2 + 4\gamma_3^2\sigma^2 - 4\gamma_2\Delta - 8\gamma_2\gamma_5 - 8\gamma_3\gamma_1\sigma + 4\gamma_1^2 + 4\gamma_2^2 + 4\gamma_0^2\sigma^2 + 16\gamma_4^2\sigma^2, \tag{A30}$$

$$D = 4\gamma_1\Delta + 8\gamma_1\gamma_5 - 8\gamma_3\gamma_5\sigma - 8\gamma_1\gamma_2 + 8\gamma_2\gamma_3\sigma - 4\Delta\gamma_3\sigma - 16\gamma_0\gamma_4\sigma^2. \tag{A31}$$

A naive comparison between the energies along the ΓK line in both models would give $\gamma_i' = \gamma_i$ and $\Delta' = \Delta$ (except for $\gamma_4' = -\gamma_4$). However this choice would only be correct along this line, from the results along the *HKH* line we know already that Δ', γ_2', and γ_5' fulfil a different relation. If we take these results into account, we find

$$\gamma_0' = \gamma_0, \tag{A32}$$

$$\gamma_3' = \gamma_3, \tag{A33}$$

$$\gamma_4' = -\gamma_4. \tag{A34}$$

Note the $-$ sign in front of γ_4.

*Electronic address: bart.partoens@ua.ac.be
†Electronic address: francois.peeters@ua.ac.be

[1] D. D. L. Chung, J. Mater. Sci. **37**, 1475 (2002).
[2] K. S. Novoselov, A. K. Geim, S. V. Morozov, D. Jiang, Y. Zhang, S. V. Dubonos, I. V. Grigorieva, and A. A. Firsov, Science **306**, 666 (2004).
[3] K. S. Novoselov, A. K. Geim, S. V. Morozov, D. Jiang, M. I. Katsnelson, I. V. Grigorieva, S. V. Dubonos, and A. A. Firsov, Nature (London) **438**, 197 (2005).
[4] Y. B. Zhang, Y.-W. Tan, H. L. Stormer, and Ph. Kim, Nature (London) **438**, 201 (2005).
[5] V. P. Gusynin and S. G. Sharapov, Phys. Rev. Lett. **95**, 146801 (2005).
[6] N. M. R. Peres, F. Guinea, and A. H. Castro Neto, Phys. Rev. B **73**, 125411 (2006).
[7] E. McCann and V. I. Fal'ko, Phys. Rev. Lett. **96**, 086805 (2006).
[8] K. S. Novoselov, E. McCann, S. V. Morozov, V. I. Fal'ko, M. I. Katsnelson, U. Zeitler, D. Jiang, F. Schedin, and A. K. Geim, Nat. Phys. **2**, 177 (2006).
[9] S. B. Trickey, F. Müller-Plathe, G. H. F. Diercksen, and J. C. Boettger, Phys. Rev. B **45**, 4460 (1992).
[10] P. R. Wallace, Phys. Rev. **71**, 622 (1947).
[11] R. Saito, G. Dresselhaus, and M. S. Dresselhaus, *Physical Properties of Carbon Nanotubes* (Imperial, London, 1998).
[12] J. C. Slonczewski and P. R. Weiss, Phys. Rev. **109**, 272 (1958).
[13] J. W. McClure, Phys. Rev. **108**, 612 (1957).